DOI: 10.1002/mds3.10167

RESEARCH ARTICLE



3D printing of polymeric Coatings on AZ31 Mg alloy Substrate for Corrosion Protection of biomedical implants

Eben Adarkwa | Ruben Kotoka | Salil Desai

Center of Excellence in Product Design and Advanced Manufacturing, North Carolina A&T State University, Greensboro, NC, USA

Correspondence

Salil Desai, Center of Excellence in Product Design and Advanced Manufacturing, North Carolina A&T State University, 422-B McNair Hall, 1601, East Market Street, Greensboro, NC 27411, USA.

Email: sdesai@ncat.edu

Abstract

Magnesium (Mg) alloys show promise in biomedical implants due to their excellent mechanical strength, biocompatibility and biodegradability. However, their rapid degradation rates in vivo induce toxicity and reduce their mechanical strength thereby, limiting their widespread usage. Our group employs a 3D inkjet printing technique for polymeric surface modification of bioresorbable AZ31 Mg alloy towards corrosion control. Thin films of three proprietary formulations of elastomeric poly (ester urethane) urea (PEUU) embedded with an anti-proliferative drug paclitaxel (Taxol) were coated on biodegradable AZ31 Mg coupons. Multilayer coatings of 5 and 20 layers were deposited for virgin (PEUU-V), PEUU with phosphorylcholine (PEUU-PC) and PEUU with sulfobetaine (PEUU-SB). Coating thicknesses of 8 μm and 19 μm were observed for 5-layer and 20-layer coatings, respectively. Surface morphology results depicted the presence of Taxol beads on PEUU-V and PEUU-SB coatings due to precipitation. An equivalent circuit model was used to calculate the polarization resistance values and revealed that the polymeric coatings provided a significant protective effect on the corrosion rate of AZ31 Mg alloy. Electrochemical impedance spectroscopy measurements indicated that PEUU-SB offered the least resistance to corrosion and had the highest porosity (35.6%) among all the polymeric coatings. PEEU-V polymeric coatings offered the greatest polarization resistance with the least porosity (10.5%). Statistical analysis confirmed that the 20-layer coating thickness had a significantly higher polarization resistance than the 5-layer coatings. This research lays the foundation for developing corrosion control drug-eluting coatings for cardiovascular and other medical device applications via surface modification using 3D inkjet printing.

KEYWORDS

3D printing, corrosion control, electrochemical impedance spectroscopy, magnesium alloys, polymeric coatings

INTRODUCTION

Metallic biomaterials have traditionally been used for implant devices due to their corrosion resistance properties in the body (Zheng et al., 2014). However, recently, a new class of biodegradable materials has

evolved, thereby expanding the traditional paradigm as an alternative for medical implant devices (Desai et al., 2008, 2021; Desai & Shankar, 2021). Magnesium (Mg) and its alloys have attracted considerable research interest for biomedical applications because of their promising properties such as biocompatibility, low density, high specific strength, castability, and appropriate hardness (Cheng et al., 2013; Gao et al., 2009; Li et al., 2019; Shashikala et al., 2008; Wu et al., 2006; Zhang et al., 2012, 2013). However, the high corrosion rate of Mg severely limits its usage in almost all of these applications (Gray & Luan, 2002; Tan et al., 2013). Therefore, in order to utilize Mg in these applications, the corrosion rate of Mg needs to be modulated (Hornberger et al., 2012; Witte, 2010). An effective way to reduce the corrosion rate of Mg and its alloys is surface modification (Gray & Luan, 2002; Hornberger et al., 2012; Lu et al., 2012). Often, surface modification is done on medical implants to enhance surface texture, biocompatibility, wear resistance and corrosion resistance (Deutchman et al., 2009; Kappelt et al., 2007; Perkins et al., 2014, 2015; Tang, 2004).

To change the surface characteristics of implant materials, various surface modification techniques have been developed thus far (Desai & Harrison, 2010; Desai, Perkins et al., 2010; Marquetti & Desai, 2018a,b, 2019). The implementation of multilayered coatings has proven effective in providing corrosion control and tunable release of different healing agents when encapsulated within bioresorbable polymeric thin films (Aikawa, 1978; Brar et al., 2009; Rude, 1998). The problems associated with conventional polymer/drug loading coating techniques such as spraying, dipping and electrospinning have been discussed extensively by De Gans et al. (2004). They range from the incapability to firmly control and maintain drug concentration, variations and inconsistency in drug concentration from device to device, recurrent webbing between the struts, inability to vary drug distribution in a controlled and predetermined manner for a more desirable drug loading profile and inability to control the local density of the drug. Furthermore, inability to spatially control and issues with cost also exist as wastage of very expensive active compounds during coating is a major problem with most of these conventional techniques. The use of the drop-on-demand inkjet printing eliminates the issues associated with conventional coating techniques and offers numerous advantages as discussed by Cooley et al. (2002). As stated by Cooley et al. 'Inkjet based deposition requires no tooling, is non-contact, and is data-driven; no masks or screens are required; the printing information is created directly from CAD information stored digitally. Being data-driven, it is flexible. As a coating and additive process with no chemical waste, it is environmentally friendly and cost effective'. The major advantages of an inkjet stent coating technique stem from its excellent process control, reproducible nature of the droplets and precise deposition onto the medical device (Cooley, Wallace, & Antohe, 2016; Tarcha et al., 2007). Its ability to produce very complex coatings is also commendable (Adarkwa et al., 2014; Izabele & Desai, 2018; Perkins et al., 2011; Xu et al., 2014). Thus, different polymer/drug combinations can be used in solutions to form multilayered coatings. The local thickness or density of the polymer/drug can be varied to achieve different release kinetics behaviours at specific locations. It offers an exclusive advantage for coating miniature and complex medical devices like stent with drugs/polymer combinations in cases where the active drug is very expensive, and wastage is not tolerated (Tarcha et al., 2007). In recent years, 3D printing technology has

been implemented in biomanufacturing of coatings and scaffolds (Aljohani & Desai, 2018; Desai et al., 2009; Desai, Richardson, et al., 2010 Parupelli & Desai, 2019).

To address the need for biodegradable and non-thrombogenic coatings for corrosion control, different formulations of elastomeric polymers were considered. Three different proprietary formulations of elastomeric polymers were synthesized and obtained from the University of Pittsburgh, PA (Wagner Lab), for corrosion control and as a carrier for anti-proliferation drug Taxol. These include poly(ester urethane) urea virgin (PEUU-V), poly(ester urethane) urea with phosphorylcholine (PEUU-PC) and poly(ester urethane) urea with sulfobetaine (PEUU-SB) containing non-thrombogenic groups. Phosphorous and sulfobetaine containing PEUU has recently been the subject of extensive research in the biomedical field (De Gans et al., 2004; Desai & Shankar, 2008). This is in part due to their superior properties such as biocompatibility, hemocompatibility, protein adsorption resistance and drug loading capacity over traditional PLA, PGLA and PCL. Additionally, their ability to flex around medical devices of various shapes and forms make them a preferred polymeric candidate over traditionally rigid polymers. The PEUU-PC and PEUU-SB used for the coating fabrication were synthesized at the University of Pittsburgh, PA (Wagner Lab), according to the processes stated by Hong et al. (2012) and Ye et al. (2014). This research aims to evaluate the corrosion resistance properties of these proprietary engineered polymers on AZ31 Mg alloy using 3D inkjet printing as a method of surface coating and modification.

2 | METHODOLOGY

2.1 | Materials

AZ31 alloy plates were acquired from Alfa Aesar and used as coating substrates. Samples were cut into 10 mm × 10 mm coupons, cleaned and used as coating substrates. Three different proprietary formulations of elastomeric poly(ester urethane) urea (PEUU-V), poly(ester urethane) urea with phosphorylcholine (PEUU-PC) (Hong et al., 2012), and poly(ester urethane) urea with sulfobetaine (PEUU-SB) Ye et al. (2014) were synthesized and obtained from University of Pittsburgh, PA (Wagner Lab). These polymers contained non-thrombogenic groups for corrosion control and as a carrier for anti-proliferation drug taxol. Paclitaxel drug (Taxol drug, LC Laboratories, PA) was used as a model drug known for its anti-proliferative and anti-inflammatory characteristics which can prevent restenosis after angioplasty. The 2, 2, 2-trifluoroethanol (TFE) obtained from Aldrich, Allentown, PA, was used as a solvent for dissolution.

2.2 | Substrate cleaning procedure

AZ31 alloy coupons underwent a pre-cleaning procedure and were mechanically polished progressively. The pre-cleaning treatment involved an initial rinsing of the substrates with ethanol to remove organic surface impurities followed by further rinsing with excess ethanol. The rinsed substrates were then cleaned by etching in 3 mol/L of nitric acid solution. Substrates were washed with excess acetone and then sonicated in acetone for 10 min to remove the acids on the surface. The mechanical polishing process consisted of the use of 320, 600 and 1200 grit SiC polishing paper progressively to eliminate surface adhered impurities. The polished substrates were rinsed, sonicated in acetone for 10 min, and stored in fresh acetone before coating.

2.3 | Coating solution preparation

The various coating polymeric solutions were prepared by dissolving the three biopolymers (PEUU-V, PEUU-PC, and PEUU-SB) and paclitaxel (5 wt% of polymer) in separate quantities of 2, 2, 2-trifluoroethanol (TFE) solvent purchased from Aldrich, Allentown, PA, to obtain a 1% w/v solution of the polymeric candidates. These polymeric solutions were then sonicated for 20 minutes to help aid a homogeneous mixture and further filtered using a 30-µm pore size filter to remove any debris. The polymeric solution concentration (1% w/v) chosen for this research was based on preliminary trials conducted with various polymeric solution concentrations to ascertain the best fit for jettability. Polymeric solutions of 1% w/v concentration were found to be the highest concentration capable of being 3D printed. The polymeric coating was provided to act as a barrier layer to retard the rapid corrosion of AZ31 alloy.

2.4 | Coating procedure

The JetLab® 4 Drop-on-Demand (DOD) 3D Inkjet Printing System (MicroFab Technologies Inc., Plano, Texas, USA) was employed for coating the polished AZ31 alloy substrates with the different polymeric solutions. A printing nozzle with an orifice dimension of 50 µm

was used for all the printing procedures. A motion controller printing script was coded for uniformly coating each substrate. The substrate temperature was controlled at 20°C. Uniform coatings of 5 and 20 layers were printed on the substrates. Figure 1 shows the custom 3D direct-write printing equipment and schematic for depositing the polymeric formulations on the substrates.

2.5 | Design of experiments

The experimental design for the corrosion control studies is shown in Table 1. Coating thickness was varied at 5 and 20 layers, Taxol concentration was fixed at 5 wt% of polymer, and the polymeric solution concentration was also fixed at 1 wt% of polymer in solvent. The run sequence for the coating process was determined randomly and each experimental run was replicated five times (n = 5). One sample set was used for the uncoated bare AZ31 magnesium coupon. Thus, a total of thirty-five (N = 35) samples were prepared for the corrosion studies. Three replicates (n = 3) were used for corrosion testing, whereas two replicates (n = 2) were used for adhesion, scanning electron microscopy (SEM), and surface morphological testing.

2.6 Coating morphology characterization

The morphology of the different coatings samples fabricated was analysed using a scanning electron microscope (SEM) Hitachi SU8000. Depending on the particular sample being analysed, an acceleration voltage ranging from 5 to 10 kV was used to capture high-quality images. SEM was used to qualitatively characterize surface morphology on various coating samples before the corrosion test. The samples used for SEM analysis were coated with Palladium (Pd) using a sputter coater system to obtain a conductive surface and reduce the incidence of charging due to the high negative charges accumulating on the sample surface. SEM was also used to examine



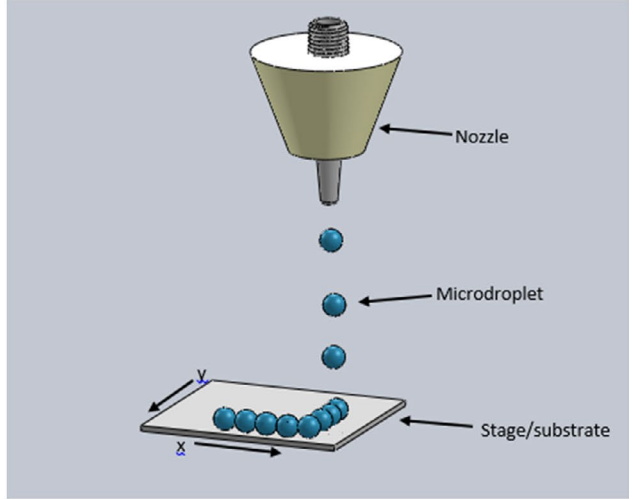


FIGURE 1 Schematic of the custom 3D printing equipment for deposition of polymeric formulations on AZ31 alloy substrate

TABLE 1 Sample description and experimental condition

Run/Sample No.	Polymer Type	Coating Thickness (Layers)
1	Bare AZ31	0 (uncoated)
2	PEUU-V	5
3	PEUU-V	20
4	PEUU-SB	5
5	PEUU-SB	20
6	PEUU-PC	5
7	PEUU-PC	20

the nano-composite structure inside the dried polymeric coating surface.

2.7 | Adhesion test

The adhesion of any coating on the substrate is an extremely critical factor in determining the quality of the coating for its proper applications (Gupta et al., 2013; Valli, 1986). Low-quality films could peel off from the substrate and hence are of little importance towards their beneficial application for substrate. The adhesion of the polymeric coatings to the Mg substrate was evaluated according to the American Society for Testing Materials (ASTM) (Mittal, 1978). ASTM-D3359-02 tape test was chosen to study the adhesion of polymeric coatings on the Mg alloy substrates. In this test, a crosscut pattern of 1 mm separation distance was made on the coated samples. An ASTM standard pressure-sensitive tape was firmly adhered

onto the coatings and then removed according to the procedure as described in the ASTM tape adhesion test.

2.8 | Corrosion test

The effect of different polymeric material and coating thickness on the corrosion polarization resistance of AZ31 Mg alloy substrates was analysed using electrochemical impedance spectroscopic measurement technique (EIS) measurements. According to Cano et al. (2010), EIS is an important electrochemical technique used for the study of coatings for metallic corrosion. EIS measurements were performed in Gibco Hank's balanced salt solution (HBSS) using a Gamry Potentiostat (R600, Gamry Instruments) at room temperature and a pH of 7.4. The choice of HBSS was based on an extensive literature review as it is the predominantly used solution for in vitro corrosion test for cardiovascular devices. HBSS was used to simulate the normal ion concentration under physiological tissue conditions. A standard three-electrode configuration consisting of Ag/AgCl electrode and platinum wire was used as the reference and counter electrodes, respectively. Fabricated polymeric-coated AZ31 Mg alloy samples were used as working electrodes. EIS measurements were performed in a frequency of 10⁰ to 10⁶ Hz using the Gamry R600 Potentiostat at the open circuit potential with a sinusoidal voltage of amplitude 10 mV. The resulting sinusoidal current was measured at the platinum counter electrode. The samples were immersed in the test solution for 15 minutes until steady-state conditions were achieved before commencing the experiments. Fresh HBSS solution was used for each experiment. The analysis presented in this research was performed using ECHEM ANALYST commercial software

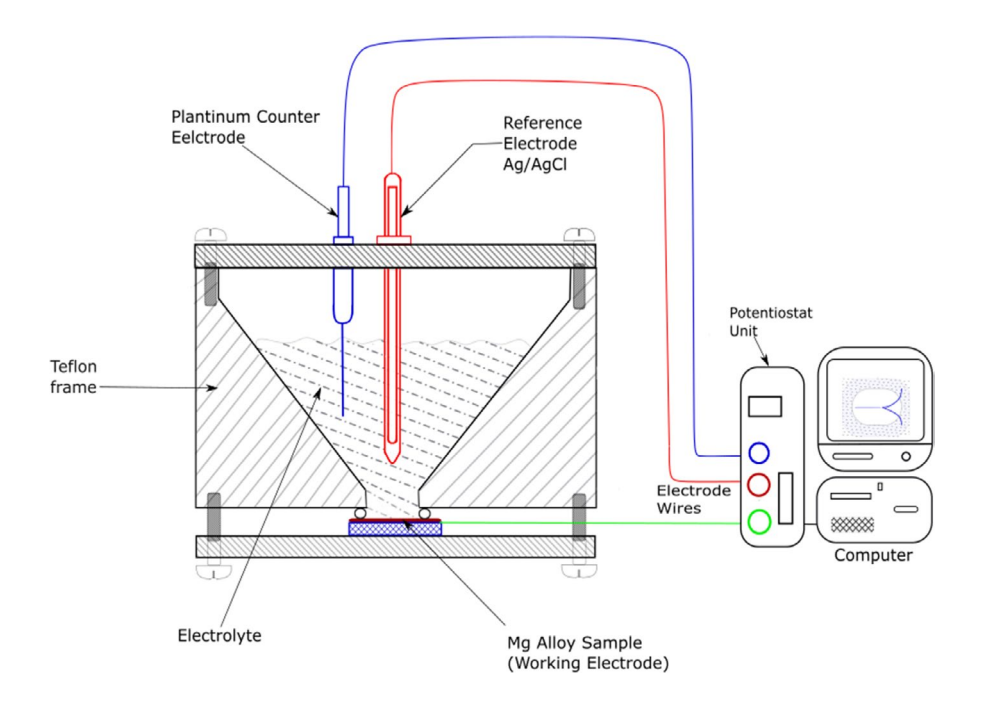
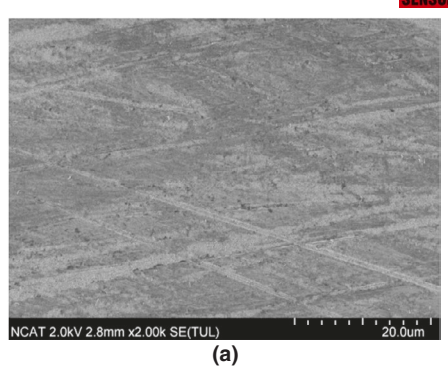


FIGURE 2 Schematic of the experimental setup for electrochemical corrosion testing



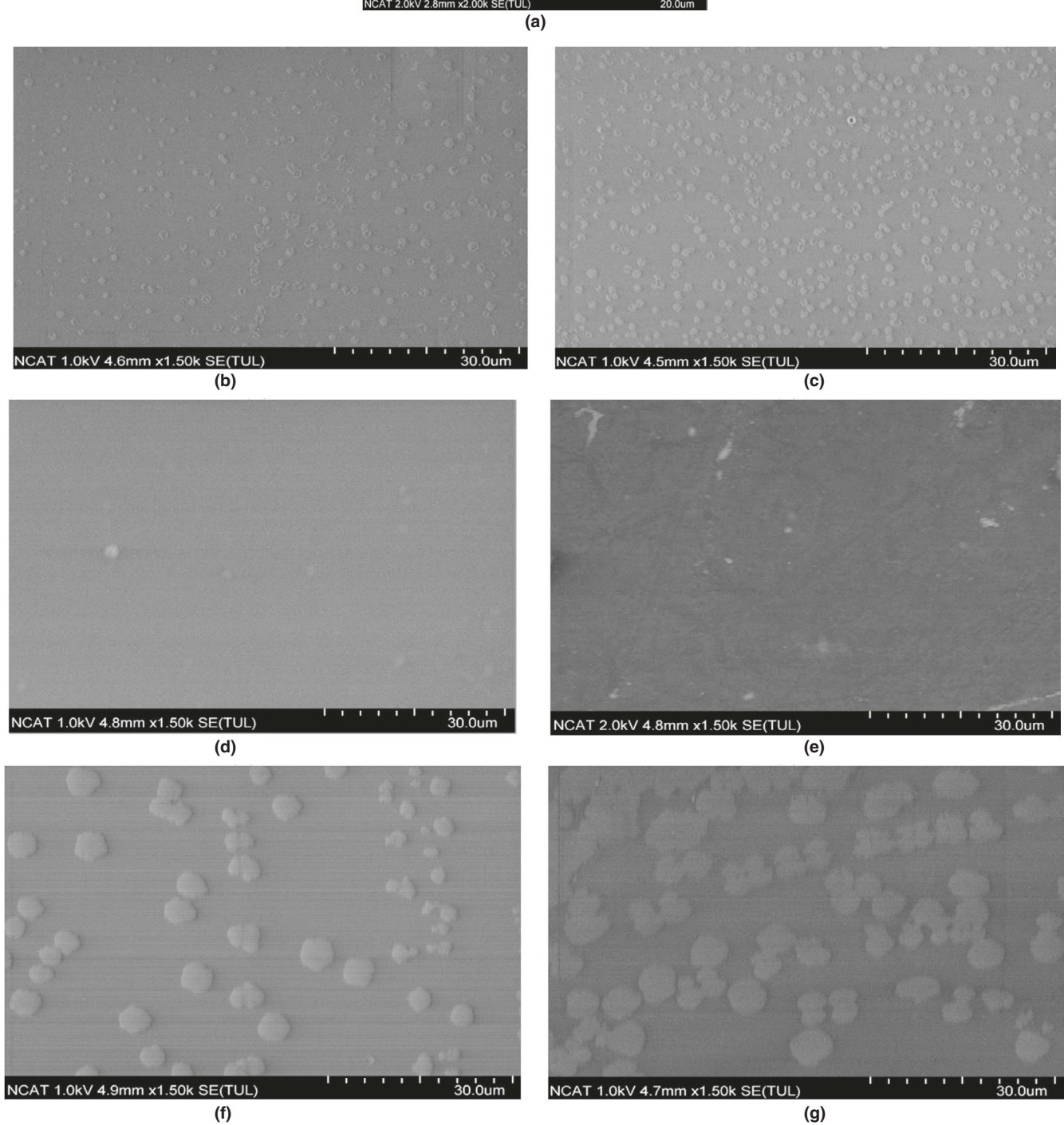
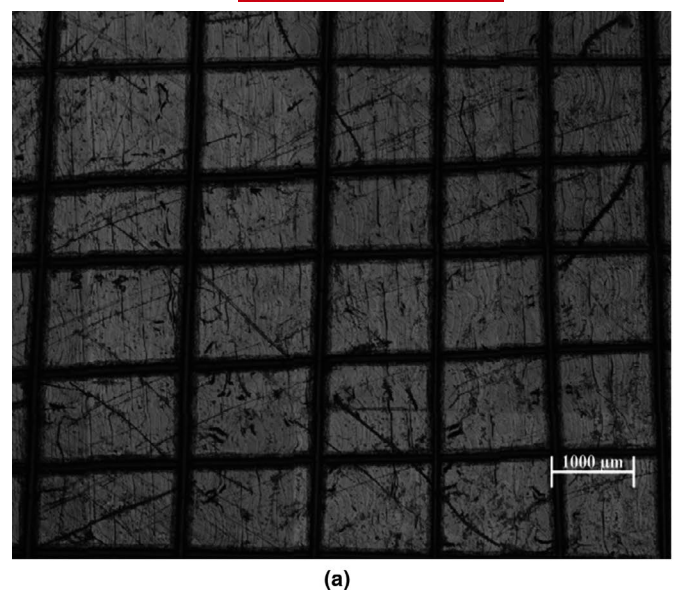


FIGURE 3 SEM image of (a) mechanically polished bare AZ31 Mg alloy substrate, PEUU-V coatings with (b) 5 layers and (c) 20 layers, PEUU-PC coatings with (d) 5 layers and (e) 20 layers, PEUU-SB coatings with (f) 5-layers and (g) 20-layers



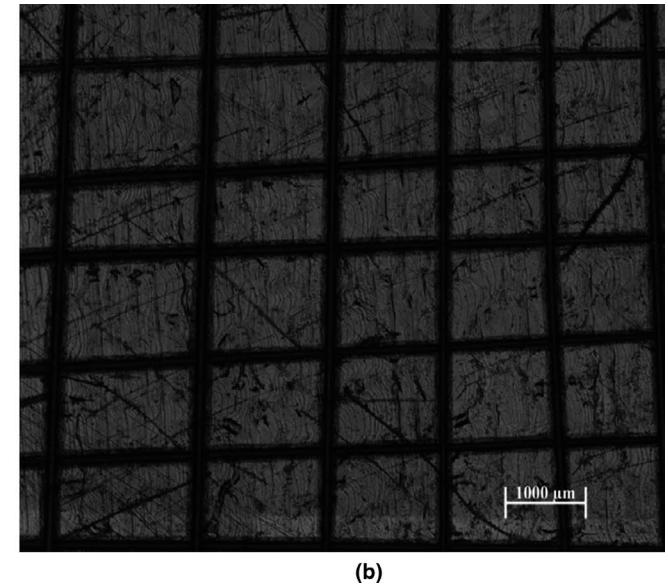


FIGURE 4 Optical images of PEUU-V 5-layer coatings (a) before and (b) after adhesion test

developed by Gamry. Figure 2 illustrates the experimental setup for the electrochemical corrosion test used in this research.

2.9 | Statistical analysis

Statistical analysis using analysis of variance (ANOVA) technique was employed to ascertain the significance of each experimental run on the response variable (polarization resistance). Three set of hypotheses were formulated below:

$$\mbox{Set 1:} \begin{cases} H_0 = \mbox{There is no interaction effect between Polymer and Coating Thickness} \\ H_1 = \mbox{There is interaction effect between Polymer and Coating Thickness} \end{cases}$$

Set 2:
$$\begin{cases} H_0 = \text{There is no main Polymer effect} \\ H_1 = \text{There is main Polymer effect} \end{cases}$$

Set 3:
$$\begin{cases} H_0 = \text{There is no main Coating Thickness} \\ H_1 = \text{There is main Coating Thickness} \end{cases}$$

3 | RESULTS AND DISCUSSION

3.1 | Coating integrity and morphological characterization

The microstructures of the fabricated polymeric coatings were studied using scanning electron microscopy. This technique was used to visualize mechanically polished bare AZ31 Mg alloy samples as well as fabricated coating film samples. The SEM image of mechanically polished bare AZ31 Mg alloy substrate using 1200 SiC grit paper is

shown in Figure 3a. Surface morphology of the coated substrates revealed that the mechanical polishing marks as seen on the bare AZ31 Mg alloy substrate were completely covered by the different polymeric coatings. Substrates coated with PEUU blends displayed dispersed raster spots of Taxol drug. These raster pattern spots are precipitated Taxol beads in both the 5 layers and the 20 layers as shown in Figure 3b and c. These findings are similar as shown by Perkins et al. (2014). SEM images obtained for PEUU-PC polymeric coatings showed a comparatively smoother surface coating with less Taxol precipitations as shown in Figure 3d and e. This homogenous mixture is due to the high drug loading capacity of the synthesized PEUU-PC as proven by Hong et al. (2012). PEUU-SB polymeric coatings Figure 3f and g also displayed relatively larger size beads of precipitated Taxol 3. Furthermore, these taxol beads tend to coagulate towards each other rather than the uniformly dispersed pattern seen with the PEUU coatings.

3.2 | Adhesion test

The adhesion of the polymeric coatings to the AZ31 Mg alloy substrate was evaluated according to the American Society for Testing Materials (ASTM) (Mittal, 1978). ASTM-D3359-02 tape test was chosen to study the adhesion of the various polymeric coatings on AZ31 Mg alloy substrates. A lattice pattern with 7-9 cuts in each direction was made in the polymeric film to the substrate. Pressure-sensitive tape was then applied over the lattice and then peeled off. Adhesion was evaluated by comparison with descriptions and illustrations as stated by the ASTM D3359-02 procedure (ASTM International, 2017). Optical images obtained before and after applying the pressure-sensitive tape to the polymeric-coated samples depicted coatings that were undetached from the substrates. This indicates a strong adhesion between polymeric coatings and

AZ31 Mg alloy substrate. Figure 4 shows an optical image before and after adhesion test for PEUU-V-coated samples.

As seen in the optical images after adhesion test, all the coating was undetached after the removal of the pressure-sensitive tape from the coated sample. A classification of '5B' (0% area removed) was assigned as the adhesion test results for each sample fabricated. This indicated that the polymeric coatings strongly adhered on the surface of the AZ31 Mg alloy substrate.

3.3 | Coating thickness and surface profile

Coating thickness was evaluated using the Alpha-Step IQ surface profilometer. Polymeric films were cut to reveal the cross-sectional and thickness profiles. The average coating thickness for 20-layer coatings was estimated at 19 μm whereas that for a 5-layer coating film was estimated at 8 μm . Since these two coating layer levels gave distinct differences in thickness measurement, the effect of coating layers/thickness on corrosion rate can be ascertained via statistical analysis. Surface morphology of the coatings was studied, and polymeric coatings had variations in their topography for both 5- and

20-layer coatings. A screenshot from the Alpha-Step IQ surface profilometer for PEUU-PC 5-layers is shown in Figure 5.

3.4 | Electrochemical testing

The electrochemical impedance spectroscopy (EIS) was used as the primary technique to characterize the corrosion protection performance of the polymeric coatings. The corrosion resistance of the various polymeric coatings in Hanks solution media was studied using the EIS analysis. These experiments were conducted using the Gamry Potentiostat (R600, Gamry® Instrument). In the EIS studies, the experimental setup consisted of an electrolyte solution (Hank's balanced salt solution), a reference electrode (standard Ag/AgCl electrode), a counter electrode (platinum wire) and the coated sample of interest which acted as the working electrode. EIS measurements were recorded at the open circuit potential. Figure 6 shows the Nyquist plots for the uncoated AZ31 and the various polymeric coating samples with 20 and 5 layers. As seen in the Nyquist plot, the real and imaginary part of the impedance increases with a decrease in the frequency.

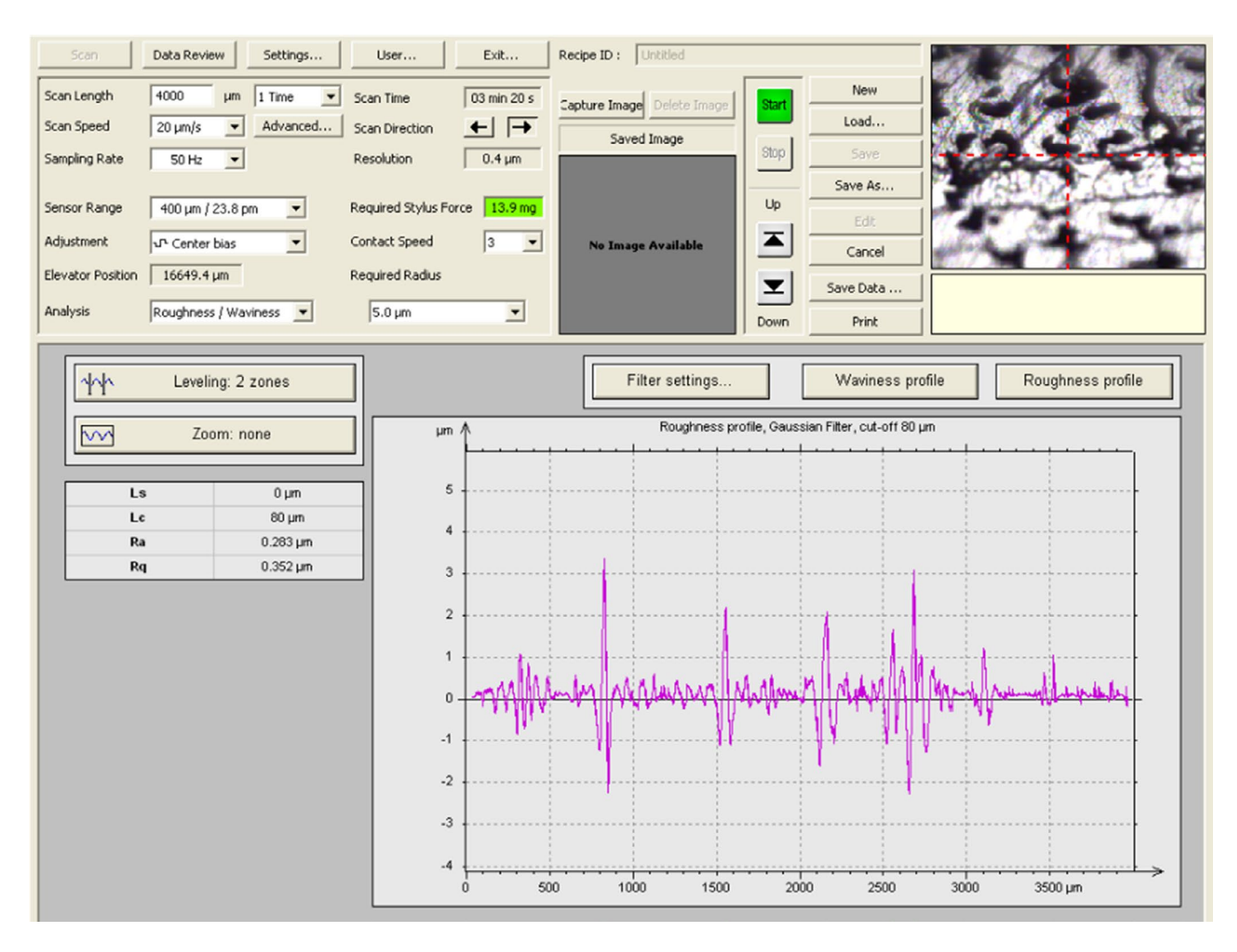


FIGURE 5 Surface roughness test output for PEUU-PC 5-layers

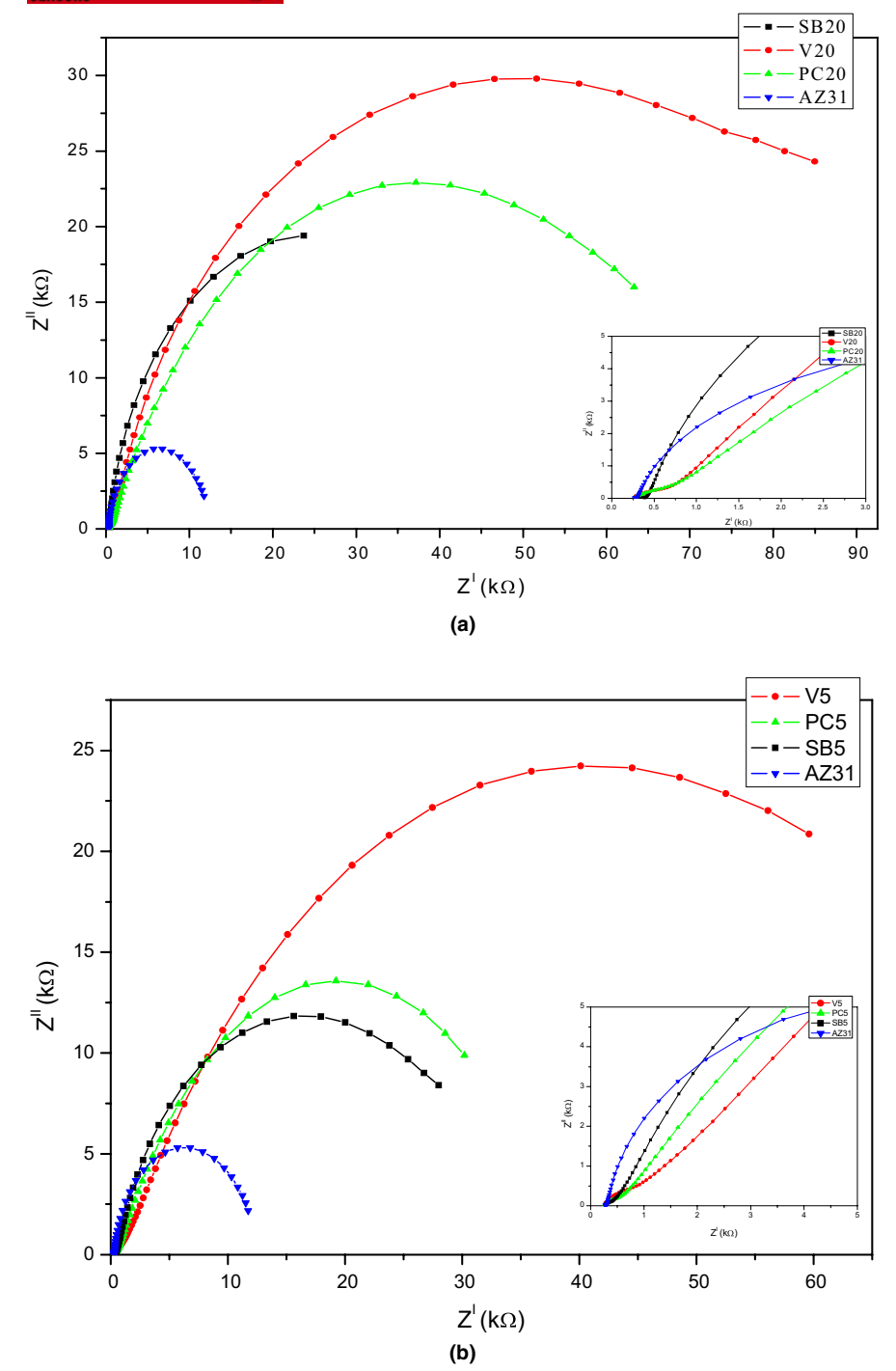


FIGURE 6 Nyquist plot for bare and polymeric-coated AZ31 samples (a) 20 layer and (b) 5 layer

The corrosion resistance of the various samples was estimated as a function of the diameter of the semicircles shown in Figure 6. The smaller the diameter, the lower the resistance to corrosion, and hence, the higher the corrosion rate. As seen in Figure 6, the corrosion resistance of the polymeric-coated AZ31 substrates is much higher than the bare AZ31 Mg alloy substrate. The observed impedance shows that the corrosion resistance increases in this order; uncoated AZ31 < PEUU-SB < PEUU-PC < PEEU-V for both 20- and

5-layer polymeric coatings. A comparative analysis each polymeric coating and layers is in Figure 7.

Although a side-by-side comparison of 5- and 20-layer coatings from Figure 7 depicts a significant difference in corrosion resistance of the various polymeric coatings, a modelled data coupled with statistical analysis was used to ascertain this. The corrosion resistance of the various polymeric coatings was also studied using the Bode plot. In the Bode plot, the coated AZ31 samples had higher

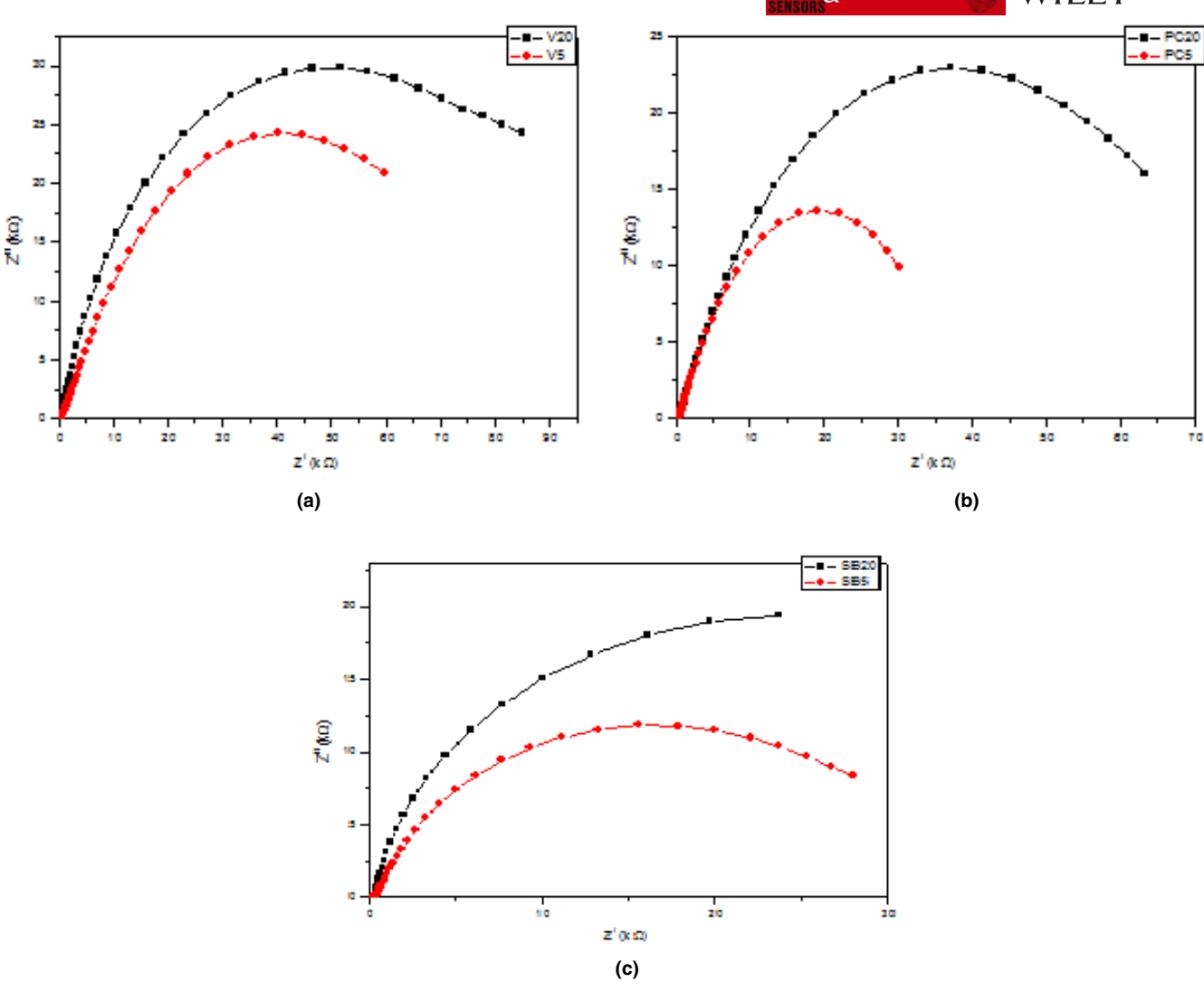


FIGURE 7 Nyquist plot for 5- and 20-layer coatings (a) PEUU-V, (b) PEUU-PC and (c) PEUU-SB50

impedance as compared to the uncoated Mg sample as seen in Figure 8. The higher value of impedance further confirms the corrosion protective nature of the various polymeric coatings for AZ31 samples. These impedance values are directly related to the corrosion resistance of the polymeric materials.

The observed impedance from the Bode plots shows that the corrosion resistance increases in this order; bare AZ31 < PEUU-SB < PEUU-PC < PEEU-V for both 20- and 5-layer polymeric coatings. The polymeric coatings with 20-layers were seen to offer better corrosion resistance properties than their corresponding 5-layer coatings.

3.5 | Equivalent circuit modelling

Detailed interpretation of the EIS plots was performed by numerical simulation using an equivalent circuit modelling (ECM). The analysis of impedance data requires appropriate models based on

the physical and chemical properties of the system under study. In equivalent circuit modelling, the response of the electrochemical system was modelled by a network of resistors, capacitors and inductors (passive circuit elements) which mimics the physical and electrochemical properties of the system. Most impedance data reported in literature for polymer-coated substrates (Hu et al., 2012; Mansfeld, 1995; Montemor & Ferreira, 2007) validate the proposed circuit model as shown in Figure 9. The analysis presented was performed using ECHEM analyst commercial software developed by Gamry[®]. This software uses a complex non-linear least-square fitting procedure of several iterations to mimic the experimental data while varying the parameters to minimize the error between the fitted result and the experimental data.

The equivalent circuit model comprised of solution resistance (R_s), coating resistance ($R_{\rm coat}$), constant phase element of the coated structure (CPE $_{\rm coat}$), electron transfer resistance ($R_{\rm et}$) and constant phase element of double-layer capacitance (CPE $_{\rm dl}$). For AZ31 samples, a magnesium hydroxide layer is naturally formed and was

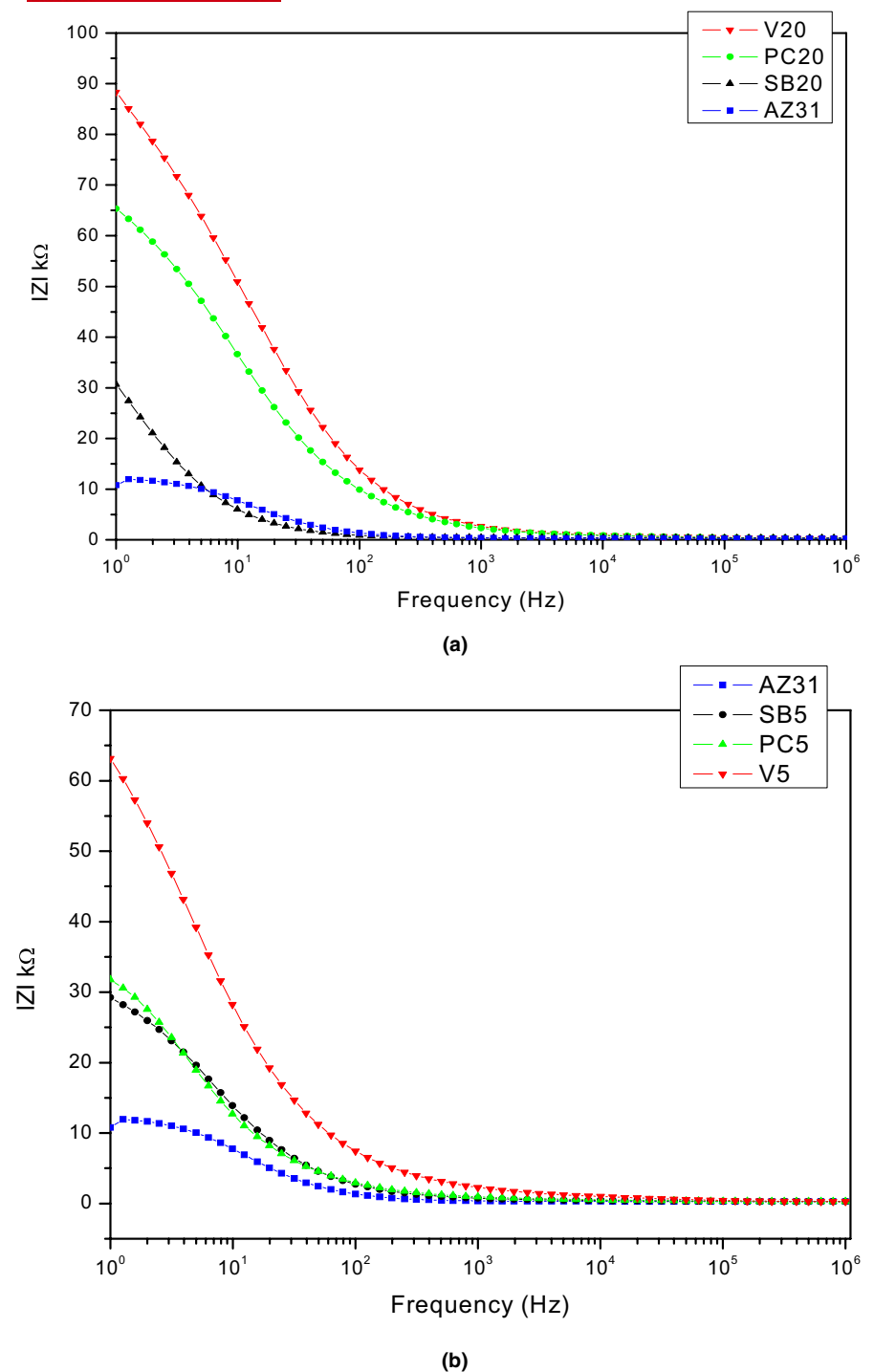


FIGURE 8 Bode plots for different samples with (a) 20-layer and (b) 5-layer coatings

modelled as a new time constant (CPE $_{\rm coat}$, corresponding capacitance) and magnesium hydroxide resistance ($R_{\rm coat}$), respectively. In the case of various polymeric-coated AZ31 samples, $R_{\rm coat}$ and CPE $_{\rm coat}$ were utilized as corrosion resistance coating layers. The summation of $R_{\rm coat}$ and $R_{\rm et}$ for each sample is indicative of the corrosion resistance of the sample.

The coating resistances ($R_{\rm coat}$, n=3 median) and the electron transfer resistance ($R_{\rm et}$, n=3 median) obtained using the modelled equivalent circuit for Figures 9 and 10 are summarized in Table 2 for

each experimental run. It is evident that the summation of $R_{\rm coat}$ and $R_{\rm et}$ for each of the polymeric-coated AZ31 substrates was markedly higher than that of bare AZ31 Mg alloy substrate. Similarly, 20-layer coating thickness provided a higher corrosion resistance than their corresponding 5-layer coatings. From the graphical representation as shown in Figure 10, the corrosion resistance increases in the same order as discussed previously. Statistical analysis was performed on the obtained numerical results to ascertain the statistical significance between the different coating layers.

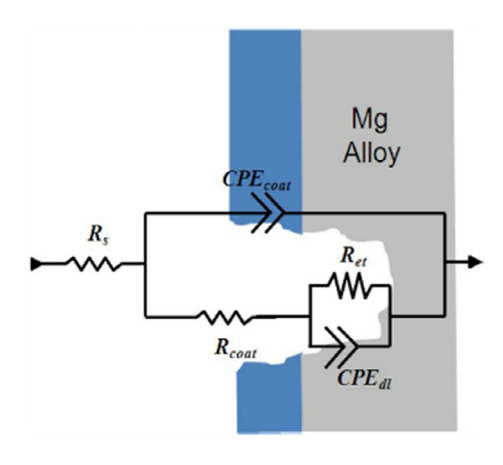


FIGURE 9 Equivalent circuit model used for fitting experimental EIS spectra

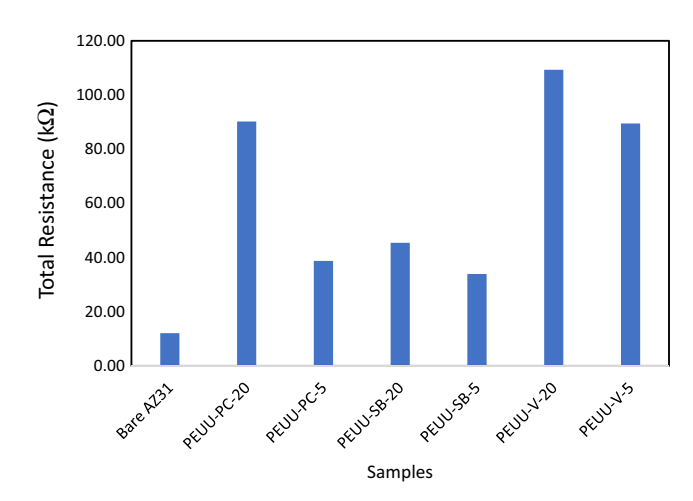


FIGURE 10 Total corrosion resistance for bare AZ31 and polymeric-coated AZ31 samples

3.6 | Porosity and protection efficiency of the coatings equivalent

The porosity of the coating is another important parameter for determining the corrosion protective nature of the coating for any substrate. For porous polymeric coatings, the pores provide direct path between the corrosive media and the substrate leading to localized corrosion of the substrate. This form of corrosion has been reported to accelerate the corrosion of the substrate, in the case of magnesium causing hydrogen embritlement (Song & Atrens, 2003). The more porous the polymeric coatings are, the faster their degradation and corrosion rate since most of these biodegradable polymers undergo hydrolytic degradation. The porosity of the protective coating was estimated using equation 1 as proposed by Creus et al. (2000).

$$P = \left(\frac{R_{ps}}{R_p}\right) \times 10^{-(\Delta E_{corr}/b_A)}$$
 (1)

The total coating porosity rate is denoted by P whereas R_{ps} is the polarization resistance of the uncoated AZ31 substrate and R_{n}

TABLE 2 Summary of EIS results for bare and coated AZ31 samples obtained from the ECM

	Parameters	
Samples	R _{coat} (Ω)	$R_{\rm et}(\Omega)$
Bare AZ31	2.28	12060.00
PEUU-PC-20	19350.00	70850.00
PEUU-PC-5	8574.00	30145.2
PEUU-SB-20	23140.00	22280.00
PEUU-SB-5	7560.00	26400.00
PEUU-V-20	50300.00	59000.00
PEUU-V-5	42230.00	47230.00

is the polarization resistance of the various polymeric-coated AZ31 sample. $\Delta E_{\rm corr}$ is the difference in potential between the corrosion potentials of the coated substrate and uncoated substrate, and $b_{\rm A}$ is the anodic Tafel slope for the uncoated substrate.

The porosity results as shown in Figure 11 can be correlated to the corrosion resistance plots as shown in Figure 10. It can be deduced that, the more porous the polymeric coatings are, the less the corrosion resistance, hence, the higher the corrosion rate. The most porous coating was PEUU-SB-5 which offered the least corrosion resistance protection properties. PEUU-V-20 had the least porosity percentage and thus offered the greatest corrosion resistance of all the polymeric coatings.

3.7 | Statistical analysis of modelled EIS data

Statistical analysis using analysis of variance (ANOVA) technique was employed to ascertain the statistical significance of each experimental run on the response variable (corrosion resistance) for each experimental sample. Using the corrosion polarization resistance data for each experimental run obtained from the equivalent circuit model, SAS 9.3 statistical software was used to analyse the corrosion resistance data. Below are the set of hypotheses to be tested.

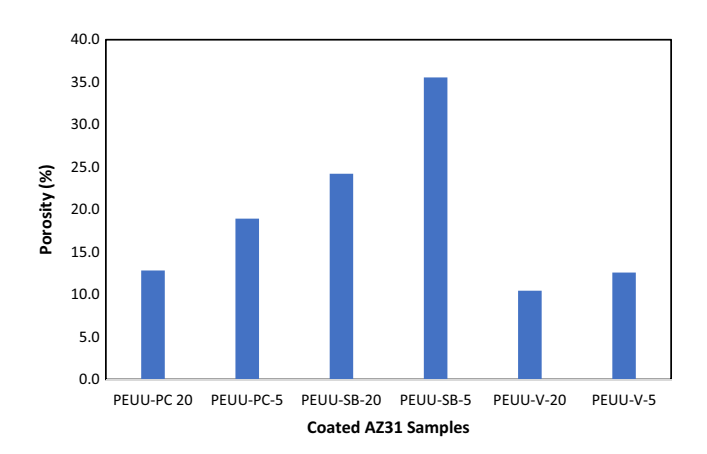


FIGURE 11 Percentage porosity of the various polymeric coatings

Test for Normality						
Test	Statistic		p Value			
Shapiro-Wilk	W	0.963553	Pr < W	.6714		
Kolmogorov-Smirnov	D	0.143748	Pr > D	>.1500		
Cramer-von Mises	W-Sq	0.043844	Pr > W-Sq	>.2500		
Anderson-Darling	A-Sq	0.265472	Pr > A-Sq	>.2500		

TABLE 3 Output for test of normality.

Set 1:
$$\begin{cases} H_0 = \text{There is no interaction effect between Polymer and Coating Thickness} \\ H_1 = \text{There is interaction effect between Polymer and Coating Thickness} \end{cases}$$

Set 2:
$$\begin{cases} H_0 = \text{There is no main Polymer effect} \\ H_1 = \text{There is main Polymer effect} \end{cases}$$

Set 3:
$$\begin{cases} H_0 = \text{There is no main Coating Thickness} \\ H_1 = \text{There is main Coating Thickness} \end{cases}$$

Before ANOVA was used, model adequacy was checked. The residual plots (normality, independence and variance) from SAS output indicated no violation. Furthermore, the test for normality was confirmed with the Shapiro-Wilk test. The null hypothesis for the Shapiro-Wilk test is that the data are normally distributed. The p-value (0.6714) was greater than the significant level (α) of 0.05 as shown in Table 3. Thus, the null hypothesis was not rejected and there is enough evidence to conclude that the data is normally distributed.

From Table 4, a hypothesis testing was conducted for both interaction and main effects. Higher order (PolymerType*CoatingThickness) interaction effect was analysed first. At 0.05 significant level (α), since p-value (<.0001) < α (0.05), there is sufficient evidence to conclude that there exists interaction effect between the polymer type

and coating thickness on corrosion resistance. Since there exists a statistically significant interaction effect between polymer type and coating thickness, the main effect may not be valid as this interaction effect might affect those results. Hence, simple main effect was analysed by slicing. Tables 5 and 6 depict SAS output for slicing.

In analysing simple main effects, when polymer type is fixed at PEUU-PC, PEUU-SB and PEUU-V levels, respectively, it can be concluded that there exists a significant main effect for coating thickness since p-value (<.0001) < α (0.05) for all three levels.

Similarly, when coating thickness is fixed at 5 and 20 levels, respectively, there is a significant main effect for polymer type since p-value (<.0001) < α (0.05) for all the two levels. To further validate the significant difference between the various treatment levels on corrosion resistance, a pairwise comparison using Ismeans with pdiff option was conducted. The SAS output for pairwise comparison as shown in Table 7 indicates there is significant difference between various treatment levels. At a 0.05 significant level, when PEUU-PC is held constant at a 5-coating thickness, there is enough evidence to conclude that it has a significant difference with PEUU-PC 20 coating thickness, PEUU-SB 20 coating thickness, PEUU-V 5 coating thickness and PEUU-V 20 coating thickness. Similarly, at a 0.05 significant level, when PEUU-PC is held constant at a 20-coating thickness, there is enough evidence to conclude that it has a significant difference with PEUU-SB _5 coating thickness, PEUU-SB_20 coating thickness and PEUU-V 20 coating thickness. Furthermore, at a 0.05 significant level, when PEUU-SB is held constant at 5 coating

TABLE 4 ANOVA GLM procedure output.

The GLM Procedure							
Source	df	Sum of squares	Mean square	F Value	Pr > <i>F</i>		
Model	5	15247237980	3049447596	519.79	<.0001		
Error	12	70400461	5866705				
Corrected Total	17	15317638442					
Source	DF	Type I SS	Mean square	F Value	Pr > <i>F</i>		
PolymerType	2	10583215319	5291607659	901.97	<.0001		
CoatingThickness	1	3634548541	3634548541	619.52	<.0001		
PolymerTy*CoatingThi	2	1029474121	514737061	87.74	<.0001		
Source	df	Type III SS	Mean square	F Value	Pr > <i>F</i>		
PolymerType	2	10583215319	5291607659	901.97	<.0001		
CoatingThickness	1	3634548541	3634548541	619.52	<.0001		
PolymerTy*CoatingThi	2	1029474121	514737061	87.74	<.0001		



TABLE 5 Interaction effect sliced by polymer type for resistance

PolymerTy*CoatingThi Effect Sliced by PolymerType for Resistance					
PolymerType	df	Sum of Squares	Mean square	F Value	Pr > F
PEUU-PC	1	3612288067	3612288067	615.73	<.0001
PEUU-SB	1	264272067	264272067	45.05	<.0001

TABLE 6 Interaction effect sliced by coating thickness for resistance.

PolymerTy*CoatingThi Effect Sliced by PolymerType for Resistance					
CoatingThickness	df	Sum of squares	Mean square	F Value	Pr > <i>F</i>
5	2	5409789018	2704894509	461.06	<.0001
20	2	6202900422	3101450211	528.65	<.0001

TABLE 7 Output for pairwise comparison using Ismeans

The GLM Proce	edure						
Lease Squares I	Means						
PolymerType		CoatingThickness		Resistance LSMEAN		LSMEA	AN Number
PEUU-PC		5		39860	1		
PEUU-PC		20		88933.333		2	
PEUU-SB		5		35683.333		3	
PEUU-SB		20		49856.667		4	
PEUU-V		2		89654.333		5	
PEUU-V		20		112566.667		6	
Lease Squares I	Means for effect F	PolymerTy*CoatingThi					
Pr > t for H0: I	LSMean(i) = LSMe	an(j)					
Dependent Var	iable: Resistance						
i/j	1	2	3	4	5		6
1		<.0001	.0563	.0006	<.0001		<.0001
2	<.0001		<.0001	<.0001	.7218		<.0001
3	.0563	<.0001		<.0001	<.0001		<.0001
4	.0006	<.0001	<.0001		<.0001		<.0001
5	<.0001	.7218	<.0001	<.0001			<.0001
6	<.0001	<.0001	<.0001	<.0001	<.0001		

thickness, there is enough evidence to conclude that it has a significant difference with PEUU-SB_20 coating thickness, PEUU-V_5 coating thickness and PEUU-V_20 coating thickness. Also, at a 0.05 significant level, when PEUU-SB is held constant at a 20-coating thickness, there is enough evidence to conclude that it has a significant difference with PEUU-V_5 coating thickness and PEUU-V_20 coating thickness. Finally, at a 0.05 significant level, when PEUU-V is held constant at a 5-coating thickness, there is enough evidence to conclude that it has a significant difference with PEUU-V_20 coating thickness. Based on the statistical analysis conducted using ANOVA, it can be concluded that, at a 0.05 significance level, different types of polymeric coatings and coating thickness have significant effect on corrosion resistance of AZ31 Mg alloy. Thus, tunable corrosion protective coatings can be developed based on the specific requirement of the intended application.

4 | CONCLUSION

In this paper, the 3D inkjet printing technique was successfully employed to fabricate polymeric coatings using different blends of PEUU embedded with Taxol drug. Biodegradable AZ31 Mg alloy coupons were utilized as the coating substrate towards the study of corrosion control. Jetting parameters were optimized for consistent coating across all polymeric solutions. Surface morphology of the coated substrates revealed the presence of Taxol precipitates for PEUU-SB and PEUU-V coatings. Strong adhesion was recorded for all polymeric coatings with the substrate as confirmed by the ASTM-D3359-02 test. PEEU-V coatings offered the greatest polarization resistance to corrosion followed by PEUU-PC, PEUU-SB, respectively. PEUU-V 20 layers offered the highest total resistance of 109.3 $\mathrm{k}\Omega$ versus PEUU-SB 5 layers offered the lowest total resistance of 33.93 $\mathrm{k}\Omega$.

This can be correlated to the differences in the porosities of the coatings. PEUU-V had the lowest porosity and thus the highest corrosion protection as compared to PEUU-SB. The observed impedance from the Bode plots showed that the corrosion resistance increases in the order: bare AZ31 < PEUU-SB < PEUU-PC < PEEU-V for both 20- and 5-layer polymeric coatings. Normality was confirmed for the statistical analysis of all the samples using the Shapiro–Wilk test. ANOVA (α = 0.05) revealed that both the polymer blend type, coating thickness and their interaction had a significant effect on corrosion resistance of AZ31 Mg alloy. This research demonstrates that tunable corrosion protective coatings can be developed for biomedical implants by manipulating the material and process parameters.

ACKNOWLEDGEMENT

The authors would like to thank the NSF Engineering Research Center for Revolutionizing Metallic Biomaterials (NSF-EEC award 0812348) and NSF-CMMI awards (1435649 and 1663128) for support towards this research. We express our gratitude to the Wagner Laboratories (University of Pittsburgh Medical Center-McGowan Institute of Regenerative Medicine) for the polymers used in this research. The authors would also like to thank the Center of Excellence in Product Design and Advanced Manufacturing at North Carolina A&T State University.

CONFLICT OF INTEREST

The authors declare no conflict of interest.

REFERENCES

- Adarkwa, E., Desai, S., Ohodnicki, J. M., Roy, A., Lee, B., & Kumta, P. N. (2014). 64th Annual Conference and Expo of the Institute of Industrial Engineers 2014. Proceedings of a meeting held 31 May 3 June 2014, Montreal, Canada. Guan, Y. (Ed.), Vol. 1, 132–138, Institute of Industrial and Systems Engineers (IISE), Curran Associates, Inc. (Dec 2014). ISBN: 9781634393843
- Aikawa, J. K. (1978). Biochemistry and physiology of magnesium. World Review of Nutrition and Dietetics, 28, 112. https://doi.org/10.1016/b978-0-12-564202-6.50009-3
- Aljohani, A., & Desai, S. (2018). 3D printing of porous scaffolds for medical applications. *American Journal of Engineering and Applied Sciences*, 11(3), 1076–1085. https://doi.org/10.3844/ajeassp.2018.1076.1085
- Cooley, P., Wallace, D., & Antohe, B. (2002). Applications of Ink-Jet Printing Technology to BioMEMS and Microfluidic Systems. *Journal of the Association for Laboratory Automation*, 7(5), 33–39.https://doi.org/10.1016/s1535-5535-04-00214-x
- ASTM International (2017). ASTM D3359–17 Standard Test Methods for Rating Adhesion by Tape Test. ASTM International, 6, 1–9. https://doi.org/10.1520/D3359-17.
- Brar, H. S., Platt, M. O., Sarntinoranont, M., Martin, P. I., & Manuel, M. V. (2009). Magnesium as a biodegradable and bioabsorbable material for medical implants. *JOM Journal of the Minerals Metals and Materials Society*, 61(9), 31–34. https://doi.org/10.1007/s11837-009-0129-0.
- Cano, E., Lafuente, D., & Bastidas, D. M. (2010). August 11). Use of EIS for the evaluation of the protective properties of coatings for metallic cultural heritage: A review. *Journal of Solid State Electrochemistry*, 14(3), 381–391. https://doi.org/10.1007/s10008-009-0902-6

- Cheng, J., Liu, B., Wu, Y. H., & Zheng, Y. F. (2013). Comparative in vitro study on pure metals (Fe, Mn, Mg, Zn and W) as biodegradable metals. *Journal of Materials Science and Technology*, 29(7), 619–627. https://doi.org/10.1016/j.jmst.2013.03.019.
- Cooley, P., Wallace, D., & Antohe, B. (2002). Applications of Ink-Jet Printing Technology to BioMEMS and Microfluidic Systems. *JALA. Journal of the Association for Laboratory Automation*, 7(5), 33–39. https://doi.org/10.1016/s1535-5535-04-00214-x.
- Creus, J., Mazille, H., & Idrissi, H. (2000). Porosity evaluation of protective coatings onto steel, through electrochemical techniques. Surface and Coatings Technology, 130(2-3), 224-232. https://doi.org/10.1016/S0257-8972(99)00659-3.
- De Gans, B. J., Duineveld, P. C., & Schubert, U. S. (2004). Inkjet printing of polymers: State of the art and future developments. *Advanced Materials*, 16(3), 203–213. https://doi.org/10.1002/adma.200300385
- Desai, S., Bidanda, B., & Bártolo, P. (2008). Metallic and ceramic biomaterials: Current and future developments. In P. Bártolo & B. Bidanda (Eds.), *Bio-Materials and Prototyping Applications in Medicine* (pp. 1–14). Springer.
- Desai, S., Bidanda, B., & Bártolo, P. J. (2021). Emerging trends in the applications of metallic and ceramic biomaterials. In P. J. Bártolo, & B. Bidanda (Eds.), *Bio-materials and prototyping applications in medicine* (pp. 1–17). Springer International Publishing.
- Desai, S., & Harrison, B. (2010). Direct-writing of biomedia for drug delivery and tissue regeneration (pp. 71–89). Springer.
- Desai, S., Moore, A., Harrison, B., & Sankar, J. (2009). Understanding microdroplet formations for biomedical applications. In ASME International Mechanical Engineering Congress and Exposition, Proceedings (Vol. 15, pp. 119–123). American Society of Mechanical Engineers Digital Collection.
- Desai, S., Perkins, J., Harrison, B. S., & Sankar, J. (2010). Understanding release kinetics of biopolymer drug delivery microcapsules for biomedical applications. *Materials Science and Engineering B: Solid-state Materials for Advanced Technology*, 168(1), 127–131. https://doi.org/10.1016/j.mseb.2009.11.006.
- Desai, S., Richardson, A., & Lee, S. J. (2010). 60th Annual Conference and Expo of the Institute of Industrial Engineers 2010, Desc: Proceedings of a meeting held 5-9 June 2010, Cancun, Mexico.. Vol. 2, 1692-1697, ISBN: 9781632663054.
- Desai, S., & Shankar, M. R. (2008). Polymers, composites and nano biomaterials: Current and future developments. In P. Bártolo & B. Bidanda (Eds.), Bio-Materials and Prototyping Applications in Medicine (pp. 15–26). Springer.
- Desai, S., & Shankar, M. R. (2021). Emerging Trends in polymers, composites, and nano biomaterial applications. In P. J. Bártolo, & B. Bidanda (Eds.), *Bio-materials and prototyping applications in medicine* (pp. 19–34). Springer International Publishing.
- Deutchman, A. H., Partyka, R. J., & Borel, R. J. (2009). Orthopaedic implants having self-lubricated articulating surfaces designed to reduce wear, corrosion, and ion leaching. Retrieved from http://v3.espacenet.com/textdoc?DB=EPODOC&IDX=EP2296582
- Gao, L., Zhang, C., Zhang, M., Huang, X., & Jiang, X. (2009). Phytic acid conversion coating on Mg-Li alloy. *Journal of Alloys and Compounds*, 485(1–2), 789–793. https://doi.org/10.1016/j.jallcom.2009.06.089.
- Gray, J. E., & Luan, B. (2002). April 18). Protective coatings on magnesium and its alloys A critical review. *Journal of Alloys and Compounds*, 336(1-2), 88–113. https://doi.org/10.1016/S0925-8388(01)01899-0
- Gupta, R. K., Mensah-Darkwa, K., & Kumar, D. (2013). Effect of post heat treatment on corrosion resistance of phytic acid conversion coated magnesium. *Journal of Materials Science and Technology*, 29(2), 180– 186. https://doi.org/10.1016/j.jmst.2012.12.014.
- Hong, Y., Ye, S. H., Pelinescu, A. L., & Wagner, W. R. (2012). Synthesis, characterization, and paclitaxel release from a biodegradable, elastomeric, poly(ester urethane)urea bearing phosphorylcholine

- groups for reduced thrombogenicity. *Biomacromolecules*, 13(11), 3686–3694. https://doi.org/10.1021/bm301158j.
- Hornberger, H., Virtanen, S., & Boccaccini, A. R. (2012). Biomedical coatings on magnesium alloys A review. *Acta Biomaterialia*, 8(7), 2442–2455. https://doi.org/10.1016/j.actbio.2012.04.012
- Hu, R. G., Zhang, S., Bu, J. F., Lin, C. J., & Song, G. L. (2012). Recent progress in corrosion protection of magnesium alloys by organic coatings. *Progress in Organic Coatings*, 73(2-3), 129–141. https://doi.org/10.1016/j.porgcoat.2011.10.011
- Izabele, M., & Desai, S. (2018). IISE Annual Conference and Expo 2018, Desc: Proceedings of a meeting held 19-22 May 2018, Orlando, Florida, USA. Vol. 2, 1108–1113. Institute of Industrial and Systems Engineers (IISE), Curran Associates, Inc. (Nov 2018)
- Kappelt, G., Kurze, P., Banerjee, D., & Adden, N. (2007). US20100131052A1 - Method for producing a corrosion-inhibiting coating on an implant made of a biocorrodible magnesium alloy and implant produced according to the method - Google Patents. https://patents.google.com/patent/US20100131052
- Li, Z., Xiong, G., Zhang, X., Shen, Z., Luo, C., Shang, X., Wang, F. Y. (2019). A GPU based parallel genetic algorithm for the orientation optimization problem in 3d printing. In *Proceedings IEEE International Conference on Robotics and Automation* (Vol. 640, pp. 134–156). Institute of Electrical and Electronics Engineers Inc.
- Lu, Y., Tan, L., Xiang, H., Zhang, B., Yang, K., & Li, Y. (2012). Fabrication and Characterization of Ca-Mg-P Containing Coating on Pure Magnesium. *Journal of Materials Science and Technology*, 28(7), 636–641. https://doi.org/10.1016/S1005-0302(12)60109-1.
- Mansfeld, F. (1995). March). Use of electrochemical impedance spectroscopy for the study of corrosion protection by polymer coatings. *Journal of Applied Electrochemistry*, 13(4), 749–758. https://doi.org/10.1007/BF00262955
- Marquetti, I., & Desai, S. (2018a). Adsorption behavior of bone morphogenetic protein-2 on a graphite substrate for biomedical applications. American Journal of Engineering and Applied Sciences, 11(2), 1037–1044. https://doi.org/10.3844/ajeassp.2018.1037.1044.
- Marquetti, I., & Desai, S. (2018b). Molecular modeling the adsorption behavior of bone morphogenetic protein-2 on hydrophobic and hydrophilic substrates. *Chemical Physics Letters*, 706, 285–294. https://doi.org/10.1016/j.cplett.2018.06.015.
- Marquetti, I., & Desai, S. (2019). Orientation effects on the nanoscale adsorption behavior of bone morphogenetic protein-2 on hydrophilic silicon dioxide. RSC Advances, 9(2), 906–916. https://doi.org/10.1039/C8RA09165J.
- Mittal, K. (1978). Adhesion measurement of thin films, thick films, and bulk coatings. adhesion measurement of thin films, thick films, and bulk coatings. ASTM International, 640, 134–156. https://doi.org/10.1520/stp640-eb.
- Montemor, M. F., & Ferreira, M. G. S. (2007). Electrochemical study of modified bis-[triethoxysilylpropyl] tetrasulfide silane films applied on the AZ31 Mg alloy. *Electrochimica Acta*, 52(27), 7486–7495. https://doi.org/10.1016/j.electacta.2006.12.086
- Parupelli, S. K., & Desai, S. (2019). A Comprehensive review of additive manufacturing (3D Printing): Processes, applications and future potential. *American Journal of Applied Sciences*, 16(8), 244–272. https://doi.org/10.3844/ajassp.2019.244.272
- Perkins, J., Desai, S., Wagner, W., & Hong, Y. (2011). 61st Annual Conference and Expo of the Institute of Industrial Engineers 2011, Proceedings of a meeting held 21-25 May 2011, Reno, Nevada, USA. Vol. 2, 2143-2148, Institute of Industrial and Systems Engineers (IISE), Curran Associates, Inc.
- Perkins, J., Hong, Y., Ye, S.-H., Wagner, W. R., & Desai, S. (2014). Direct writing of bio-functional coatings for cardiovascular applications. *Journal of Biomedical Materials Research Part A*, 102(12), 4290– 4300. https://doi.org/10.1002/jbm.a.35105.

- Perkins, J., Xu, Z., Smith, C., Roy, A., Kumta, P. N., Waterman, J., Conklin, D., & Desai, S. (2015). Direct writing of polymeric coatings on magnesium alloy for tracheal stent applications. *Annals of Biomedical Engineering*, 43(5), 1158–1165. https://doi.org/10.1007/s10439-014-1169-3.
- Rude, R. K. (1998). Magnesium deficiency: A cause of heterogeneous disease in humans. *Journal of Bone and Mineral Research*, 13(4), 749–758. https://doi.org/10.1359/jbmr.1998.13.4.749.
- Shashikala, A. R., Umarani, R., Mayanna, S. M., & Sharma, A. K. (2008). Chemical conversion coatings on magnesium alloys A Comparative Study. *International Journal of Electrochemical Science*, 3, 993–1004.
- Song, G., & Atrens, A. (2003). Understanding magnesium corrosion—A framework for improved alloy performance. *Advanced Engineering Materials*, 5(12), 837–858. https://doi.org/10.1002/adem.200310405
- Tan, L., Yu, X., Wan, P., & Yang, K. (2013). Biodegradable Materials for Bone Repairs: A Review. Journal of Materials Science and Technology, 29(6), 503-513. https://doi.org/10.1016/j. jmst.2013.03.002.
- Tang, L. (2004). EP1778200A1 Nanocoating for improving biocompatibility of medical implants. https://patents.google.com/patent/EP1778200A1/en
- Tarcha, P. J., Verlee, D., Hui, H. W., Setesak, J., Antohe, B., Radulescu, D., & Wallace, D.(2007). The application of ink-jet technology for the coating and loading of drug-eluting stents. *Annals of Biomedical Engineering*, 35(10), 1791–1799. https://doi.org/10.1007/s10439-007-9354-2.
- Valli, J. (1986). A review of adhesion test methods for thin hard coatings. Journal of Vacuum Science & Technology A: Vacuum, Surfaces, and Films, 4(6), 3007–3014. https://doi.org/10.1116/1.573616.
- Witte, F. (2010). The history of biodegradable magnesium implants: A review. Acta Biomaterialia, 6(5), 1680–1692. https://doi.org/10.1016/j.actbio.2010.02.028.
- Wu, G., Zeng, X., Ding, W., Guo, X., & Yao, S. (2006). Characterization of ceramic PVD thin films on AZ31 magnesium alloys. *Applied Surface Science*, 252(20), 7422–7429. https://doi.org/10.1016/j.apsusc.2005.08.095
- Xu, Z., Roy, A., Kumta, P., Waterman, J., & Desai, S. (2014). Polymeric coatings for biodegradable implants. AES-ATEMA International Conference Series - Advances and Trends in Engineering Materials and their Applications, 2014, 47–50.
- Ye, S.-H., Hong, Y. I., Sakaguchi, H., Shankarraman, V., Luketich, S. K., D'Amore, A., & Wagner, W. R. (2014). Nonthrombogenic, biodegradable elastomeric polyurethanes with variable sulfobetaine content. ACS Applied Materials and Interfaces, 6(24), 22796–22806. https://doi.org/10.1021/am506998s.
- Zhang, Q., Lin, X., Qi, Z., Tan, L., Yang, K., Hu, Z., & Wang, Y. (2013). Magnesium alloy for repair of lateral tibial plateau defect in minipig model. *Journal of Materials Science and Technology*, *29*(6), 539–544. https://doi.org/10.1016/j.jmst.2013.03.003
- Zhang, Y., Ren, L., Li, M., Lin, X., Zhao, H., & Yang, K. (2012). Preliminary study on cytotoxic effect of biodegradation of magnesium on cancer cells. *Journal of Materials Science and Technology*, 28(9), 769–772. https://doi.org/10.1016/S1005-0302(12)60128-5
- Zheng, Y. F., Gu, X. N., & Witte, F. (2014). Biodegradable metals. *Materials Science and Engineering: R: Reports*, 77, 1–34. https://doi.org/10.1016/j.mser.2014.01.001.

How to cite this article: Adarkwa E, Kotoka R, Desai S. 3D printing of polymeric Coatings on AZ31 Mg alloy Substrate for Corrosion Protection of biomedical implants. *Med Devices Sens.* 2021;4:e10167. https://doi.org/10.1002/mds3.10167